University of Groningen

A Fourier Approximation Method for the Multi-Pump Multi-Piston Power Take-Off System

Wei, Yanji; Barradas Berglind, Jose de Jesus; Muhammad Zaki Almuzakki, M.; van Rooij, Marijn; Wang, Ruoqi; Jayawardhana, Bayu; Vakis, Antonis I.

[Link to publication in University of Groningen/UMCG research database](#)

OMAE2018-77498

A FOURIER APPROXIMATION METHOD FOR THE MULTI-PUMP MULTI-PISTON POWER TAKE-OFF SYSTEM

Y. Wei   J.J. Barradas-Berglind   M. Z. Almuzakki   M. van Rooij   R. Wang   B. Jayawardhana   A. I. Vakis*
Faculty of Science & Engineering, University of Groningen,
Nijenborgh 4, Groningen 9747AG, The Netherlands

ABSTRACT

In this work, a frequency-domain method for the numerical solution of the nonlinear dynamics of a wave energy converter with a pumping system is presented. To this end, a finite Fourier series is used to describe the nonlinear force components, i.e., the pumping force. The dynamics of the buoy and the piston are obtained by solving a set of linear motion equations. The numerical model is validated by comparing it with experimental results. The dynamic characteristics of the pumping system are investigated by performing a series of numerical simulations for several approximation orders under various wave conditions. The advantages and limitations of this method are also discussed in the paper. This work provides great insight into the mechanism of a WEC with a pumping unit under various sea states, which can guide the design of a multi-piston pump (MPP) system. This model will be applied to investigate the optimal configuration for the MPP system in the future.

Introduction

The recently proposed novel wave energy converter (WEC) that constitutes the core technology of the Ocean Grazer, a hybrid ocean energy collection and storage platform, has the potential to be an effective contender in the challenge of extracting energy from offshore ocean waves. The Ocean Grazer's WEC utilizes an adaptable multi-pump multi-piston power take-off (MP^{2}PTO) system that consists of a grid of interconnected floater elements (denominated a floater blanket, FB), with each floater being connected to a piston-type hydraulic pumping system (a multi-piston pump, MPP) [1]. The working principle of this WEC consists on pumping internal fluid from a lower to an upper reservoir, creating hydraulic head and storing fluid in the upper reservoir. Each pumping system consists of three differently-sized engageable pistons, thus providing adaptability to the incoming waves by being able to alternate between seven different pumping combinations. Consequently, this particular WEC can be configured to maximize the overall energy extraction for various sea states by choosing the optimal pumping combinations. A system of check-valves working together with the pumping system prevents back-flow from the upper to the lower reservoir while pumping, which essentially results in nonlinear pulse-like pumping force profiles.

In previous work, a functional scale prototype of single piston pump (SPP), the main building element of the MP^{2}PTO system, was constructed to evaluate the performance of a pumping unit [2]; furthermore, a mathematical model was proposed to investigate its mechanical efficiency. In addition, a time-domain model was developed to demonstrate the advantage of the adaptable MPP for wave energy extraction [3], and a frequency-domain model was used to investigate the hydrodynamic behaviour and performance of a FB with linear PTO system [4]. There are some limitations in our previously developed numerical models. The time-domain model can simulate the FB with the MP^{2}PTO system under various sea states; however, due to the nonlinearity of the MP^{2}PTO system, it is computationally costly, and thus not suitable to identify the optimal pumping configurations of the system. Particularly, this would be rather critical for an FB consisting of hundreds of floating elements. On the other hand, the frequency-domain model can obtain the hydrodynamic response of a FB efficiently, but it can only deal with a linear PTO system. The nonlinearity of the MP^{2}PTO system is mainly due to the pumping force, introduced by the interaction

---

*Address all correspondence to this author. Email: a.vakis@rug.nl

of the check valves and the dynamics of the pistons, being similar to a square wave. Therefore, it would be valuable to develop a computationally-efficient numerical model for an FB incorporating the nonlinear MP^{2}PTO system.

To assist in the development of WEC technologies, many numerical methods for modeling WECs have been proposed and tested by researchers [5]. The conventional numerical modeling methods taking into account nonlinearities include time-domain techniques and computational fluid dynamics(CFD), both being computationally expensive compared to the frequency-domain approach. Moreover, the optimal control of a WEC requires a fast and accurate solution for calculating the nonlinear hydrodynamics. Korde and Ringwood [6] introduced a Fourier-Galerkin direct transcription method for optimal control of WECs. In such an approach, the displacement and the PTO force are approximated by a truncated Fourier series; thus, the numerical integration of the convolution integral can be avoided when solving the motion equations, which significantly reduces the computational cost. This approach has been extended to the nonlinear frequency-domain model of WECs by Merigaud et al. [7]. Their simulations indicate that such an approach is superior for applications involving a large number of simulations, such as WEC parametric optimisation.

The influence of the damping profile on the WEC performance and fatigue damage was investigated by Lamont-Kane et al. [8]. The authors concluded that the mean power capture at optimum damping was not sensitive to the damping profile, but the use of Coulomb damping significantly decreased the fatigue damage. Nevertheless, its influence on the dynamic response of the WEC was not discussed. Our proposed WEC system is analogous to the mechanical system of a harmonically excited oscillator incorporating Coulomb-type friction, which has been investigated by [9, 10]. Their analytical and numerical results show that a symmetric motion of the oscillator would be found with the assumption that there are only two stops per period, but the asymmetric motion might occur when this assumption was not fulfilled. The previous hints to similar phenomena possibly existing in the MP^{2}PTO system as well. Note that multiple turnarounds of the piston per period mean that the check valves may open/close frequently, which may in turn result in significant volumetric losses. Hence, it is important to investigate the system dynamics at various configurations, in order to obtain an optimal design.

The present work proposes a frequency-domain model for a single buoy with a pumping unit (i.e., an MPP), using the Fourier approximation method. Firstly, we describe the numerical model and its solution; next, we validate the model by comparing it against the SPP experiment. Subsequently, we investigate the response behaviour of the WEC when incorporating the SPP.
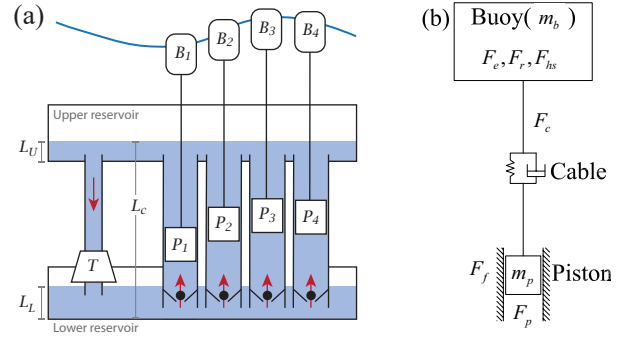
(a)

(b)

FIGURE 1: The Ocean Grazer WEC concept(a) and the schematic diagram of numerical model for a WEC with a pumping unit(b).

Numerical model

A schematic representation of the Ocean Grazer WEC is shown in Fig. 1(a). The floating elements $B_1 - B_4$ are interconnected into a "floater blanket"; each element is linked with the (multi-piston) pumping system $P_1 - P_4$ through cables. The pistons are driven by the heaving motion of the floating elements, therefore pumping water from the lower reservoir into the upper reservoir. The stored potential energy is then transformed into electricity by means of a hydraulic turbine T. This mechanical system of one floating element with a piston pump can be simplified into the lumped-element model as shown in Fig. 1(b). The buoy and piston are considered as two mass bodies, and the connecting cable is assumed to be a spring-damper element. Thus, the complete buoy-piston system is governed by the motion equations:

$$\boldsymbol{M}_b\left(\ddot{\boldsymbol{X}}_b + g\right) = \boldsymbol{F}_e + \boldsymbol{F}_r + \boldsymbol{F}_{hs} + \boldsymbol{F}_c \tag{1}$$

$$m_p\left(\ddot{z}_p + g\right) = F_p + F_f - F_{c,3} \tag{2}$$

where $\boldsymbol{M}_b \in \mathbb{R}^{6\times6}$ is a diagonal matrix of masses and moments of inertia for the general case of a buoy with 6 DOF, $\boldsymbol{X}_b \in \mathbb{R}^6$ is the displacement vector of the buoy, and $\boldsymbol{F}_e$, $\boldsymbol{F}_r$, $\boldsymbol{F}_{hs}$ and $\boldsymbol{F}_c \in \mathbb{R}^6$ represent the vectors of excitation, radiation, hydrostatic restoring and cable forces, respectively. In addition, m_p is the mass of the piston, z_p is its displacement, F_p is the pumping force due to the pressure difference between two ends of the piston, F_f is the friction between the piston and cylinder, and $F_{c,3} = \begin{bmatrix} 0 & 0 & 1 & 0 & 0 & 0 \end{bmatrix} \boldsymbol{F}_c$ is the cable force in the heaving direction.

For the SPP model, the pumping force depends on the open area of the check valve and the dynamics of the piston [1]. It can be very large during the upstroke, but becomes zero during the downstroke, which introduces a nonlinearity into the WEC system. Due to the variation of the water levels in both reser-

voirs being very small in a short period, the water levels can be assumed to be constant during one pumping cycle. Then, the pumping force can be expressed as:

$$F_p = A_t \left[\rho g \left(L_c + L_U - L_L \right) + \rho \left(L_c + L_U \right) \ddot{z}_p + \rho \dot{z}_p^2 \right], \quad (3)$$

where A_t is the time variation of the open area of the check valve, L_c is the length of the cylinder between both reservoirs, L_U and L_L are the water depth of the upper and lower reservoirs and ρ is the density of the working fluid. The first term inside the brackets in Eq. (3) represents the pressure due to the hydraulic head between two reservoirs; the second term accounts for the inertia of the working fluid in the cylinder; and the third term describes the dynamic pressure of the working fluid. Based on the parameters in [1], a scale analysis indicates that the last two terms are generally much smaller than the first term, except under high frequency waves.

Furthermore, applying the Couette flow assumption, the viscous friction force F_f acting on the piston in (2) can be described as

$$F_f = \frac{\mu \ell_p \dot{z}_p}{s_p}, \quad (4)$$

where μ is the dynamic viscosity of the working fluid, s_p is the piston-casing separation and $\ell_p = 2\pi R_p H_p$ corresponds to the lateral area of the piston with radius R_p and height H_p.

In general terms, the dynamics governing the opening and closing of the check valve should be considered in (3). Accordingly, in this work we model them by assuming that the open area of the check valve is a logistic function of the piston velocity, namely

$$A_t = \frac{A_c}{1 + e^{k(\dot{z}_p - \dot{z}_{p0})}}, \quad (5)$$

where A_c is the piston cross-sectional area, $\dot{z}_{p0}$ is the threshold piston velocity that makes the check valve half open, and k is the steepness coefficient. In the present study we use $\dot{z}_{p0} = 0$ and a smaller value of k for the opening than closing to match the measurements in the SPP experiment.

The finite Fourier series method is applied to approximate the nonlinear dynamics of the WEC system. Therefore, the free water surface elevation, as well as the displacements of buoy and piston are described as a truncated Fourier series:

$$\eta(t) = \sum_{n=0}^{N} \Re \left\{ \hat{A}_n e^{in\omega t} \right\} \quad (6)$$

$$\boldsymbol{X}_b(t) = \sum_{n=0}^{N} \Re \left\{ \hat{\boldsymbol{X}}_{b,n} e^{in\omega t} \right\} \quad (7)$$

$$z_p(t) = \sum_{n=0}^{N} \Re \left\{ \hat{z}_{p,n} e^{in\omega t} \right\} \quad (8)$$

for a frequency ω, where $\hat{A}_{w,n}$ represents the complex wave amplitude components obtained from a wave spectrum or a designed wave train, $\hat{\boldsymbol{X}}_{b,n}$ corresponds to the amplitude of the buoy displacement, and $\hat{z}_{p,n}$ is the amplitude of the piston displacement. The $n = 0$ component indicates the mean water level or displacements. Consequently, the forces in Eq. (1)-(2) can be written as:

$$\boldsymbol{F}_e(t) = \sum_{n=1}^{N} \Re \left\{ \hat{A}_{w,n} \hat{\boldsymbol{F}}_{e,n} e^{in\omega t} \right\} \quad (9)$$

$$\boldsymbol{F}_r(t) = \sum_{n=1}^{N} \Re \left\{ \left(n^2 \omega^2 \boldsymbol{A}_{r,n} - in\omega \boldsymbol{B}_{r,n} \right) \hat{\boldsymbol{X}}_{b,n} e^{in\omega t} \right\} \quad (10)$$

$$\boldsymbol{F}_{hs}(t) = \sum_{n=0}^{N} \Re \left\{ -\boldsymbol{K}_{hs} \hat{\boldsymbol{X}}_{b,n} e^{in\omega t} \right\} \quad (11)$$

$$\boldsymbol{F}_c(t) = \sum_{n=0}^{N} \Re \left\{ \left(-\boldsymbol{K}_c - in\omega \boldsymbol{C}_c \right) \left(\hat{\boldsymbol{X}}_{b,n} - \hat{z}_{p,n} \right) e^{in\omega t} \right\} \quad (12)$$

$$F_p(t) = \sum_{n=0}^{N} \Re \left\{ \hat{F}_{p,n} e^{in\omega t} \right\} \quad (13)$$

$$F_f(t) = \sum_{n=1}^{N} \Re \left\{ \frac{\mu \ell_p}{s_p} in\omega \hat{z}_{p,n} e^{in\omega t} \right\} \quad (14)$$

where $\hat{\boldsymbol{F}}_{e,n}$, $\boldsymbol{A}_{r,n}$ and $\boldsymbol{B}_{r,n}$ are the excitation, added mass and radiation damping at the nth harmonic frequency, respectively; $\boldsymbol{K}_{hs}$ contains the hydrostatic stiffness coefficients. They can be numerically obtained by the boundary element method. The open source code NEMOH [11] is used in the present paper. $\boldsymbol{K}_c$ and $\boldsymbol{C}_c$ are the stiffness and damping coefficients of the cable. The nth harmonic pumping force coefficients $\hat{F}_{p,n}$ can be calculated by performing the numerical integration:

$$\hat{F}_{p,n} = \frac{1}{T} \int_{t_0 - \frac{T}{2}}^{t_0 + \frac{T}{2}} F_p(\dot{z}_p, \ddot{z}_p) e^{-in\omega t} \, dt \quad (15)$$

Substituting Eqs. (9)-(14) into Eq. (1)-(2) and sorting out the terms by the order of the frequency, the system of equations (1)-(2) can be converted into a set of linearized equations over each harmonic, which can be solved easily in a conventional numerical computing environment, e.g., Matlab. Since $\hat{F}_{p,n}$ in Eq. (15) depends on the piston dynamics which are unknown in advance, a series of iterative steps is required. The results of $\hat{X}_{b,n}$ and $\hat{z}_{p,n}$ are obtained once the residuals of the pumping force are smaller than a predefined tolerance.

The leakage and volumetric losses are not accounted for in the present model, hence it is not possible to calculate the capture power of the WEC system. Alternately, we use the pumping power to assess the system performance. For the monotonous wave simulation, the pumping power can be expressed as:

$$P_p(\omega) = \frac{\omega}{2\pi} \int_0^{\frac{2\pi}{\omega}} F_p(t)\dot{z}_p(t)\mathrm{d}t. \qquad (16)$$

Considering a single WEC system excited by monotonous waves with only one degree of freedom in heave, we assume that the stiffness of the cable is infinite and the damping of the cable is neglected such that the buoy and piston move synchronously, and we neglect the last two terms in Eq. (3) such that the pumping force only depends on the sign of the velocity and the hydraulic head. Then, eqs. (1) and (2) can be reduced as:

$$\left(m_b + m_p + A_r\right)\ddot{z}_p + B_r\dot{z}_p + K_{hs}z_p =$$
$$|\hat{F}_e|\cos\left(\omega(t+t_0)\right) - \frac{A_c\rho g\left(L_c + L_U - L_L\right)}{2}\,\mathrm{sgn}(\dot{z}_p), \quad (17)$$

where m_b is the mass of the buoy, $\mathrm{sgn}(\dot{z}_p)$ denotes the sign operation of the piston velocity given by

$$\mathrm{sgn}(\dot{z}_p) = \begin{cases} 1 & \text{if } \dot{z}_p > 0 \\ [1,-1] & \text{if } \dot{z}_p = 0 \,, \\ -1 & \text{if } \dot{z}_p < 0 \end{cases} \qquad (18)$$

which gives the dry fiction characteristic as in [10], such that when $\dot{z}_p = 0$ the function in (18) gives undetermined values; this situation corresponds to the so-called *stick* phase when the piston is unable to move and thus sticking occurs. Comparing Eq. (17) with the motion equations of the harmonically excited dry friction oscillator (Eq. (4) in [10]), the uniqueness of the present system includes the following aspects: (1) the system has the radiation damping term; and (2) the radiation and excitation coefficients (A_r, B_r and F_e) are frequency-dependent. Therefore, this is a more complex problem than that in [10], which has not

been investigated in the context of WEC applications, using the finite Fourier approximation method.

Comparison with SPP experiment

The proposed model is validated by comparing it with the SPP experiment. In this experiment, the dynamics of the buoy are replaced by a sinusoidal oscillation provided by a motor. The details of the experimental configuration can be found in [2].

Fig. 2 shows the comparison of the pumping power as a function of the hydraulic head. The numerical results show very good agreement with those obtained in the experiment. The pumping power is almost linear to the hydraulic head, because the velocity of the piston is a semi-sinusoidal profile, and the pumping force is roughly proportional to the hydraulic head (neglecting the last two terms in Eq. (3)).
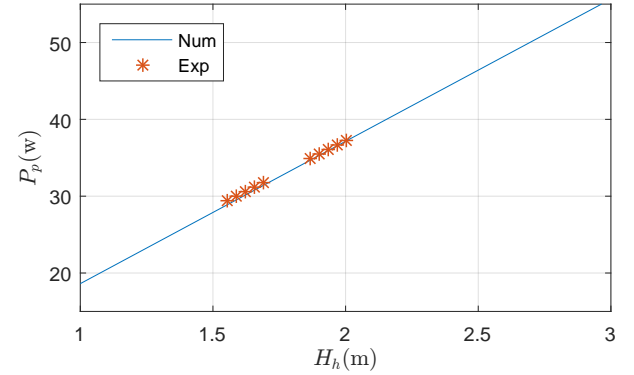

FIGURE 2: Pumping power as a function of the hydraulic head.

The comparison of the pumping power with varying periods is presented in Fig. 3. The numerical and experimental results exhibit a similar trend in the pumping power, which decreases as the period increases. The numerical model slightly underestimates the pumping power; this small difference may be caused by the phase difference between the opening and closing of the check valve, resulting in an offset in the pumping force.

The time variations of the system dynamics can be recovered from the Fourier series, which makes the numerical results directly comparable with the experimental measurements, as demonstrated in Fig. 4. There is a discrepancy in the piston displacement, appearing near the occurrence of the switching between the upstroke and downstroke, which may be caused by the inaccurate stiffness of the system in the numerical model. More specifically, the stiffness in the experiment may be multiple-factor dependent on, e.g., the supporting structure, the cable connection between the motor and piston, and the compliance of the
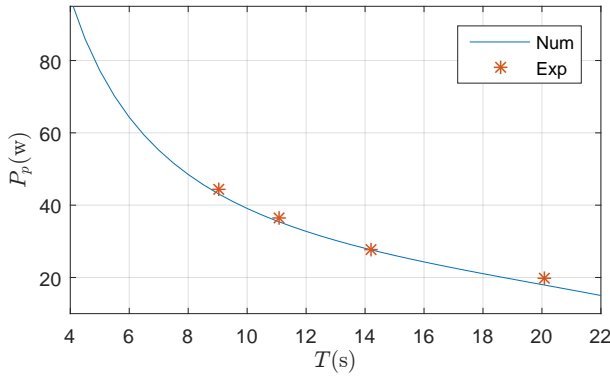
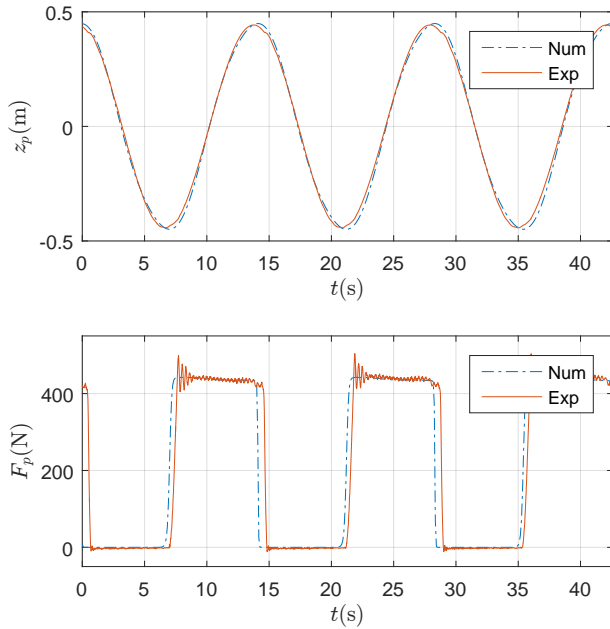**FIGURE 3**: Pumping power for different periods.

FIGURE 4: Comparison of experimental and numerical results (top: piston displacement; bottom: pumping force).

cylinder. These factors are difficult to determine and incorporate in the numerical model. A time shift is found in the pumping force, indicating that the dynamics of the check valve are not accurately described in the model (both opening/closing of the check valve occur earlier than in the experiment). We observe that this time shift is frequency dependent, implying that a more complicated expression of Eq. (5) is necessary in order to improve the accuracy of the model. This also explains why the pumping power is underestimated in Fig. 3. In addition, the high frequency oscillations of the pumping force are measured during the switching in the experiment, which is not observed

in the numerical results. Since the mathematical expression of the pumping force is a semi-discontinuous function, it is difficult to describe the mechanism during the switching. Theoretically, although the accuracy of the Fourier approximation approach depends on the choice of the order N such that one can increase N to capture this slamming phenomenon, the inherent difficulty in approximating a discontinuous function by a finite Fourier series, i.e. the Gibbs phenomenon, may affect the numerical results. Hence, this model can be used to assess the energy extraction of the pumping system, but it can hardly be applied to investigate the mechanism of the slamming.

Dynamic behaviour of the WEC with a pumping unit

After discussing the validation of the model, following our discussion on the sticking phenomena, as reported in [9], multiple sticking instances may appear when the excitation force is smaller than the maximum friction force. Analogously, in the present WEC system, sticking may occur when the wave excitation force is smaller than the pumping force. Hence, it is interesting to investigate the dynamics of the complete system by coupling the hydrodynamic force with pumping system. Accordingly, this section discusses the dynamic response and the energy extraction of the WEC coupling with a pumping unit, based on a series of numerical simulations.

It was found that the numerical results in the previous section are not sensitive to the chosen order (the higher order results are very close to those using 1st order approximation). The reason is that the motion of the buoy was replaced with a powerful motor in the experiment, which can easily overcome the pumping force. There are no sticks observed and the motion of the piston is semi-sinusoidal, but in the buoy-piston coupling system, this is not true. The convergence study is performed with various harmonic simulations. The results of the capture factor (the ratio between the pumping power of the WEC and the power of the incident wave per unit width of the device) are shown in Fig. 5. In this figure, it can be seen that the results of the 1st and 2nd order approximations are significantly different from those of higher order approximations. The lower order simulations predict higher pumping power for low frequency waves, while underestimating the power in higher frequencies. The results converge when the simulations are performed with a 3rd order approximation or higher.

The discrepancy between the simulation results with different orders is mainly caused by the appearance of sticking, which can be understood by comparing their results in the time domain in Fig. 6. In this figure, it is clear that the sticking occurs between $t = 3$ s and $t = 4$ s, and the piston keeps stationary for a while before it starts moving in the upstroke direction (Note that due to the limitation of the Fourier approximation approach, since it is impossible to obtain the explicit sticking section, i.e., $\dot{z}_p = 0$ for a certain time, we identify the piston velocity $\dot{z}_p = 0 \pm \varepsilon$ for $\varepsilon \ll 1$
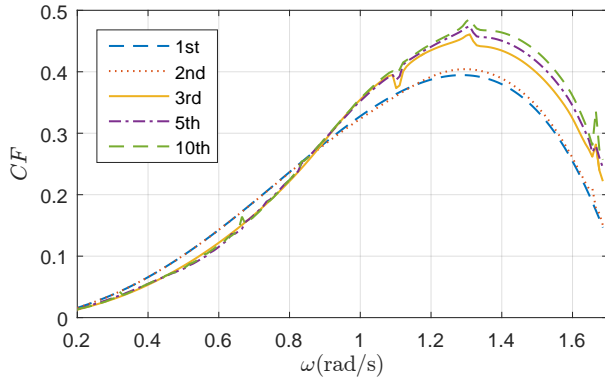
5

FIGURE 5: Capture factor profiles for different harmonic orders ($R_p = 0.3$ m, $A_w = 1$ m).

as the occurrence of the sticking). The lower order simulations i.e., the 1st and 2nd, cannot capture such a phenomenon. The results of the higher order approximation simulations show that the check valve will open and close more than once during one wave cycle, as shown in the plot of the time series of A_t, which is a major difference between the SPP experiment and the complete WEC system. Consequently, the pumping force F_p shows a similar behaviour with respect to A_t. Resultingly, the peak pumping power P_p for higher order approximation simulations is almost double that of lower order ones, as demonstrated in the last plot. In addition, we would like to remark that varying the parameters in Eq. (5) may alter the check valve dynamics, e.g., the opening/closing duration and frequency, thereby change the pumping power.

Since the present model dismisses the convolution integral or the state-space approximation for the radiation forces, it is very computationally competitive with respect to the time-domain model when choosing a proper order of the Fourier series, i.e., 3rd order approximation in the present case. This model can estimate satisfactorily the pumping power, while keeping the simulation execution efficient. The higher order simulations can describe the system dynamics better around the sticking section, but their computational cost increases dramatically due to the fact that the Fourier series of discontinuous functions will converge very slowly. The former can also be associated with the previously-mentioned Gibbs phenomenon.

In Fig. 5, it is surprising to observe several spikes occurring occasionally. Csernák et al. (2007) [10] also observed these spikes of oscillating amplitude near sub-harmonic resonance frequencies. Their interpretation is that these spikes are caused by the marginal stability of the dynamical system at those frequencies. In the present case, the spikes in the capture factor may be attributed to the sharp variation of the sub-harmonic added mass coefficient, as shown in Fig. 7. It is clear that the 1st order harmonic added mass is smooth, whereas the higher order harmonic

ones have sudden jumps at certain frequencies. These frequencies precisely coincide with the frequencies of the appearance of the spikes in Fig. 5.

Although the present model cannot accurately describe the sticking phenomenon, it can shed some light on the dynamic patterns of the system. It was reported by [10] that the number of stops per cycle is both frequency- and friction intensity-dependent. Based on a series of simulations with various radii of the piston, we obtain results exhibiting behavior similar to those in [10], which are shown in Fig. 8. These results have been converted into dimensionless quantities by:

$$S = \frac{A_c \rho g (L_c + L_U - L_L)}{2|\hat{F}_e(\omega)|} \quad (19)$$

$$t^* = t\frac{\omega}{2\pi} \quad (20)$$

$$z_p^* = z_p \frac{K_{hs}}{|\hat{F}_e(\omega)|} \quad (21)$$

$$\dot{z}_p^* = \dot{z}_p \frac{B_r(\omega)}{|\hat{F}_e(\omega)|} \quad (22)$$

where S is the ratio between the pumping force and the wave excitation, which indicates the capability for the excitation to overcome the resistance in the system. The upper and lower bounds of the shaded zone in Fig. 8 are calculated by:

$$z_s^* = \frac{\Re\left\{\hat{F}_e(\omega)e^{i\omega t}\right\}}{|\hat{F}_e(\omega)|} \pm S. \quad (23)$$

The sticking phenomenon occurs when the piston switches the moving direction in the shaded zone.

The explanation of the dynamic behaviour is the following. In the case of a low frequency incident wave, the excitation force is mainly attributed to the Froude-Krylov force, which varies slowly with the free water surface elevation. As soon as the excitation overcomes the pumping force, the piston starts to move upward. In the mean time, the buoyancy restoring force decreases, which can easily cancel the excitation force, because both forces strongly depend on the free water surface elevation. Consequently, the piston stops and will restart to move again until the excitation can overcome the pumping force. As a result, the piston sticks and the check valve closes and opens frequently. Similarly, such a mechanism may occur during the downstroke. These dynamics can be observed in Fig. 8(a), where the displacement of the piston traces the lower bound during the upstroke while tracing the upper bound during the downstroke; furthermore, the time series of piston velocity oscillates in high frequencies.

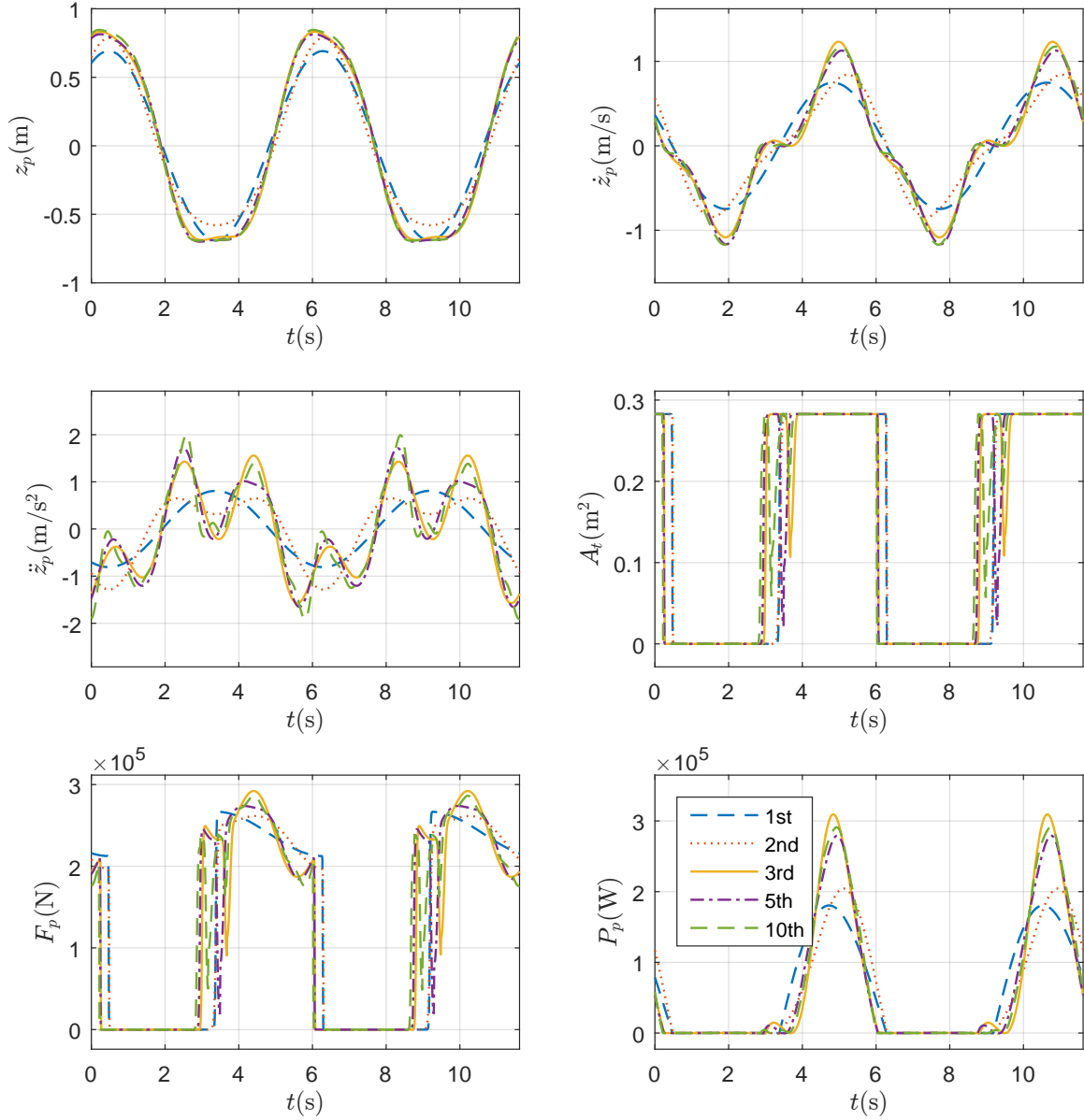When increasing the incident wave frequency, S increases

6

Copyright © 2018 by ASME

FIGURE 6: Comparison of time variation of (a) piston displacement Z_p, (b) piston velocity $\dot{Z}_p$, (c) piston acceleration $\ddot{Z}_p$, (d) open area of cylinder A_c, (e) pumping force F_p and (f) pumping power P_p ($R_p = 0.3$ m, $A_w = 1$ m, $\omega = 1.08$ rad/s).

because the excitation decreases with the wave frequency in general. A phase shift appears between the excitation force and the displacement of the piston (the shaded zone includes the phase information of the excitation force with Eq. (23)), as seen in Fig. 8(b). The two sticking sections merge and two long-duration sticking instances can be identified prior to the upstroke/downstroke.

In Fig. 8(c), it can be observed that the sticking only appears during the upstroke, and it is absent during the downstroke. The asymmetric displacement in one wave cycle may be caused by the asymmetric pumping force. The pumping force is a function of velocity and acceleration during the upstroke (the jump at the switching from downstroke to upstroke is greater than that from upstroke to downstroke), while it is constant during the downstroke, as presented in Fig. 6. As a result, it is harder for the wave excitation to overcome the pumping force in the upstroke.

The non-sticking case is not observed in the case of $R_p = 0.3$ m, when further increasing the wave frequency. Nonetheless,
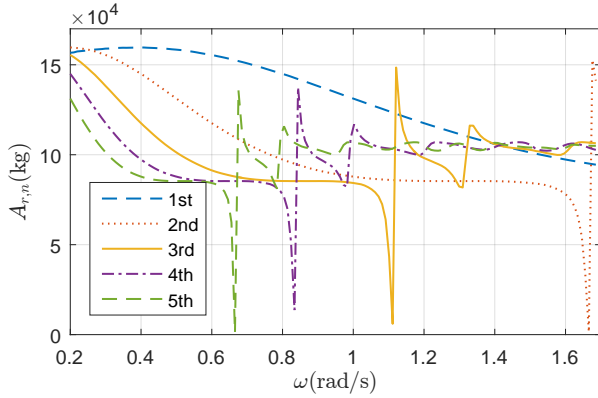
7

FIGURE 7: Sub-harmonic added mass coefficient varying with wave frequency, $A_{r,n}(\omega) = A_{r,1}(n\omega)$

it can be found in the case with a smaller piston radius (decreasing the pumping force), e.g., $R_p = 0.25$ m in Fig. 8(d). The results correspond to non-sticking semi-symmetric solutions, similar to the ones in [12, Chapter 11].

Conclusions

The present paper proposed a nonlinear frequency-domain model for a WEC with a pulse-like pumping system, based on the Fourier approximation method. Several conclusions can be drawn:

• The numerical simulations show good agreement with the SPP experiment.
• The numerical results indicate that at least 3rd order approximation is required in order to properly capture the nonlinear response and satisfactorily predict the pumping power.
• The Fourier approximation method is able to assess the energy extraction of the WEC system, but it is not very suitable to investigate the high frequency response, i.e., slamming phenomenon.
• A complete WEC system with a pumping unit behaves significantly differently than the one in the SPP experiment. Various sticking patterns may appear, depending on the incident wave frequency and the configuration of the system.

The present work placed emphasis on understanding the dynamic response of the system, while the energy extraction has not been carefully examined yet; this should be done in the future. Additionally, a more analytical approach could be taken to study the dynamic response of the system and the sticking phenomena. The current work only deals with a single buoy with one pumping unit, but it may be readily extended to an FB coupled with the MP^{2}PTO system, which is a work in progress. The present model will be applied to identify the optimal configuration of the MPP in the future.

REFERENCES

[1] Vakis, A., and Anagnostopoulos, J. S., 2016. "Mechanical design and modeling of a single-piston pump for the novel power take-off system of a wave energy converter". *Renewable Energy*, **96**, pp. 531 – 547.

[2] van Rooij, M., Meijer, H., Prins, W. A., and Vakis, A., 2015. "Experimental performance evaluation and validation of dynamical contact models of the Ocean Grazer". In OCEANS 2015 - Genova, pp. 1–6.

[3] Wei, Y., Barradas-Berglind, J., van Rooij, M., Prins, W., Jayawardhana, B., and Vakis, A., 2017. "Investigating the adaptability of the multi-pump multi-piston power take-off system for a novel wave energy converter". *Renewable Energy*, **111**, pp. 598 – 610.

[4] Wei, Y., Barradas-Berglind, J., Yu, Z., van Rooij, M., Prins, W., Jayawardhana, B., and Vakis, A., 2017. "A frequency-domain model for a novel wave energy converter". In 12th European Wave and Tidal Energy Conference (EWTEC2017).

[5] Li, Y., and Yu, Y.-H., 2012. "A synthesis of numerical methods for modeling wave energy converter-point absorbers". *Renewable and Sustainable Energy Reviews*, **16**(6), pp. 4352 – 4364.

[6] Korde, U. A., and Ringwood, J. V., 2016. *Hydrodynamic Control of Wave Energy Devices*. Cambridge University Press.

[7] Merigaud, A. P. L., and Ringwood, J. V., 2017. "A nonlinear frequency-domain approach for numerical simulation of wave energy converters". *IEEE Transactions on Sustainable Energy*.

[8] Lamont-Kane, P., Folley, M., and Whittaker, T., 2017. "The influence of pto profile on the performance and fatigue damage of wave energy converters". In Proceedings of the Twelfth European Wave and Tidal Energy Conference, A. Lewis, ed., EWTEC. ISSN: 2309-1983.

[9] Csernák, G., and Stépán, G., 2006. "On the periodic response of a harmonically excited dry friction oscillator". *Journal of Sound and Vibration*, **295**(3), pp. 649 – 658.

[10] Csernák, G., Stépán, G., and Shaw, S., 2007. "Sub-harmonic resonant solutions of a harmonically excited dry friction oscillator". *Nonlinear Dynamics*, **50**(1-2), p. 93.

[11] Babarit, A., and Delhommeau, G., 2015. "Theoretical and numerical aspects of the open source BEM solver NEMOH". In 11th European Wave and Tidal Energy Conference (EWTEC2015).

[12] Butikov, E. I., 2015. *Simulations of oscillatory systems: with awardwinning software, physics of oscillations*. Taylor & Francis Group, LLC.
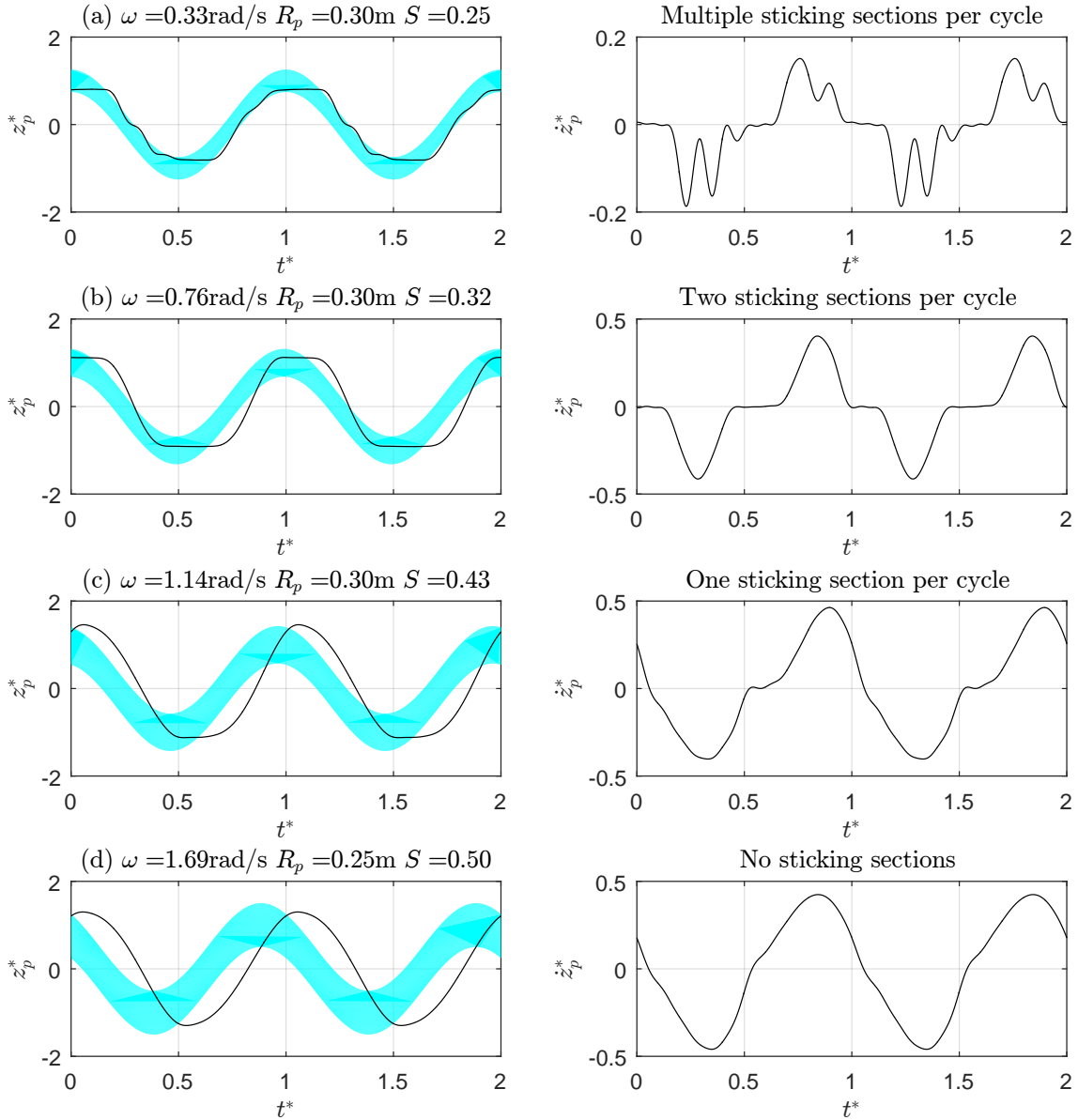
FIGURE 8: The dynamic patterns of the WEC system with various number of sticking sections per wave cycle; the plots on the left show the non-dimensional displacements of the piston, with the shaded (cyan) zones indicating the ranges that may result in sticking; the plots on the right show the non-dimensional velocity of piston. The results are derived from the simulation of the 10th order approximation.